NANO LETTERS

2008
Vol. 8, No. 2
551−557

Three-Dimensional Structure of Helical and Zigzagged Nanowires Using Electron Tomography

Han Sung Kim, Seon Oh Hwang, Yoon Myung, and Jeunghee Park*

Department of Chemistry, Korea University, Jochiwon 339-700, Korea

Seung Yong Bae

Chemical Research and Development Center, Samsung Cheil Industry Inc., Uiwang 332-2, Korea

Jae Pyoung Ahn

Advanced Analysis Center, Korea Institute of Science and Technology, Seoul 136-791, Korea

Received October 31, 2007; Revised Manuscript Received December 17, 2007

ABSTRACT

Electron tomography and high-resolution transmission electron microscopy were used to characterize the unique three-dimensional structures of helical or zigzagged GaN, $ZnGa_2O_4$, and Zn_2SnO_4 nanowires. The GaN nanowires adopt a helical structure that consists of six equivalent $\langle 0\bar{1}11\rangle$ growth directions with the axial [0001] direction. We also confirmed that the $ZnGa_2O_4$ nanosprings have four equivalent $\langle 011\rangle$ growth directions with the [001] axial direction. The zigzagged Zn_2SnO_4 nanowires consisted of linked rhombohedrons having the side edges matched to the $\langle 110\rangle$ direction and the [111] axial direction

One-dimensional (1D) nanostructures have attracted considerable attention due to their potential use as building blocks for assembling active and integrated nanosystems.[1] Recently, interest in helical (or springlike) and zigzagged nanostructures has been steadily increasing, owing to their attractive morphology and properties.[2−20] It was demonstrated that helical carbon nanotubes (CNTs) and nanowires (e.g., ZnO, InGaAs/GaAs, Cr) can be used as extremely sensitive mechanical resonators to detect mass and pressure changes.[2d,2e,5g,17,18] All of the zigzagged or helical structures in these previous studies were analyzed by examining their two-dimensional (2D) projections using transmission electron microscopy (TEM), which provides a first insight into their size and morphology. There are, however, potentially some cases where important three-dimensional (3D) structural information is missed or erroneous information may be obtained when using simply this technique.

Electron tomography, which is a method to reconstruct 3D morphologies from a series of 2D images or projections, has been successfully applied to analyze the morphology of nanoparticles as well as their location in a mesoporous matrix (or carbon nanotubes or nanocomposites).[21−28] However, the use of electron tomography to study helical or zigzagged nanowires has not previously been reported, despite the ever-increasing research effort devoted to this field. Herein, we report the 3D structures of helical or zigzagged GaN, $ZnGa_2O_4$, and Zn_2SnO_4 nanowires (NWs), obtained by electron tomography and high-resolution TEM. The present work demonstrates their 3D reconstruction images, acquired from a series of 2D projections obtained by high-angle annular dark field (HAADF) scanning TEM (STEM). The results of this study should open up a new field allowing for the investigation of nanostructures with high spatial resolution that could have an impact on our understanding of the growth mechanism and application of nanodevices in many fields in which the crystal structure plays an important role in the final properties.

The synthesis and characterization procedure of GaN and Zn_2SnO_4 NWs are described in the Supporting Information. 3D electron tomography was performed using a STEM (FEI Co., Technai F20), with a tilt holder (Dual Orientation Tomography Holder 927, Gatan Co.) and a Fischione model 3000 HAADF detector operated at 200 kV. A series of 110 HAADF-TEM images was collected from +65 to −65° in 1.5° steps under a nominal magnification of 40,000∼110,000×, resulting in a pixel size of 1∼3 nm

* Corresponding author. E-mail: parkjh@korea.ac.kr.

10.1021/nl072829i CCC: $40.75
Published on Web 01/12/2008

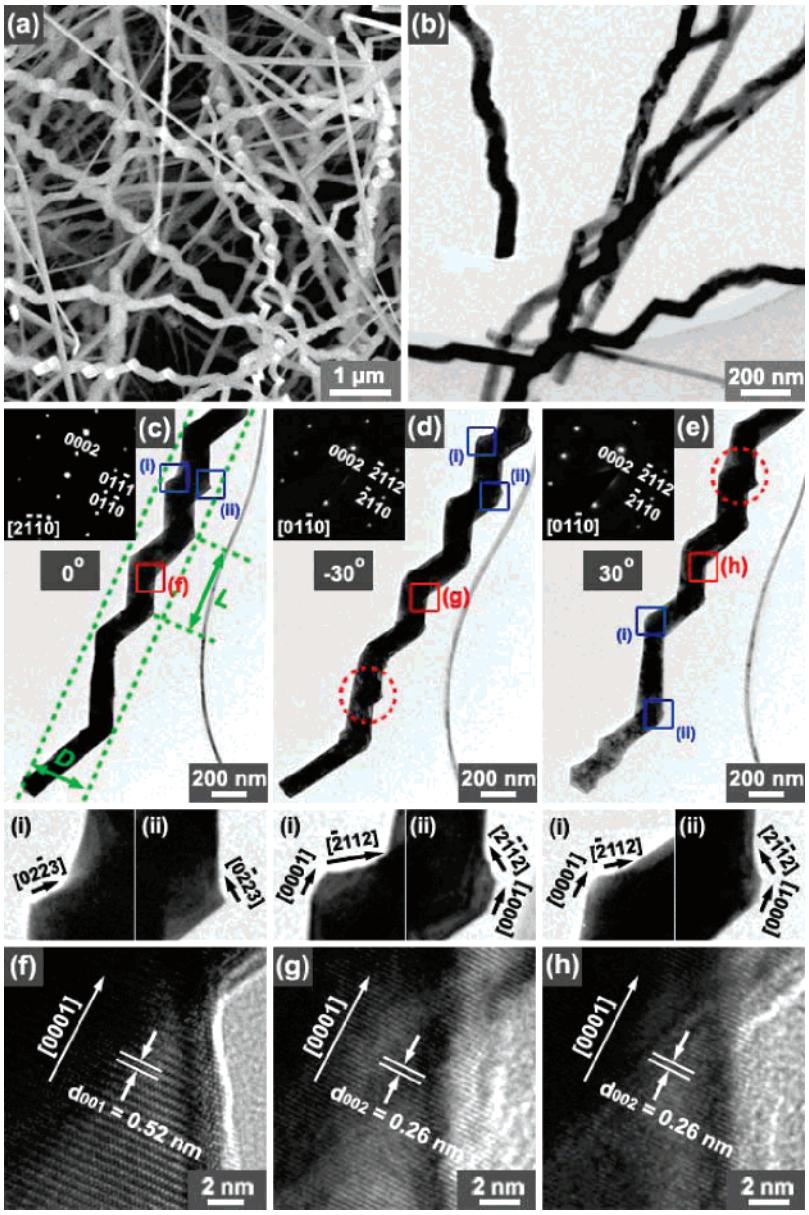

Figure 1. (a) SEM micrograph of high-density helical GaN NWs homogeneously grown on the substrate. (b) TEM image reveals the zigzagged morphology of the NWs having an average diameter of 100 nm. (c) The zigzagged NW has a pitch distance (L) in the wide range of 200−500 nm, a zigzag angle of 120−130°, and a uniform diameter of the helix (D) of about 300 nm. The insets show the SAED pattern, measured at the $[2\bar{1}\bar{1}0]$ zone axis, and the magnified images of the edge parts, revealing the $[02\bar{2}3]/[0\bar{2}23]$ zigzagged directions and the axial [0001] direction. The NW turns around the long axis by (d) −30° and (e) 30°. The corresponding SAED patterns, measured at the $[01\bar{1}0]$ zone axis, and the magnified TEM images of the left- and right-side edge parts (i and ii) show that the zigzagged direction matches the $[\bar{2}112]/[\bar{2}112]/[0001]$ directions (insets). The shorter segments appear to be nearly collinear with the others, as indicated by the circles. The lattice-resolved images for the (f) 0°-, (g) −30°-, and (h) 30°-turned NWs reveal their single-crystalline nature. The highly crystalline (001) lattice planes are separated by a distance of 5.2 Å, which is consistent with that of the bulk crystal (a = 3.189 Å, c = 5.186 Å, JCPDS no. 50-0792).

on a computer-controlled sample stage. The images were spatially aligned by a cross-correlation algorithm using Inspect3D software (FEI Co.), and the 3D reconstructions were achieved using a simultaneous iterative reconstruction algorithm from consecutive 2D slices.[29] Visualization was performed using AMIRA 4.0.

Figure 1a shows the SEM image of the high-density helical NWs synthesized using the vapor transport method. The X-ray diffraction (XRD) and X-ray photoelectron spectroscopy (XPS) data confirm the wurtzite structure GaN NWs, as shown in the Supporting Information, Figure S1. The TEM image reveals all zigzagged structure over the whole NW (Figure 1b). The average diameter (d) of the NWs is 100 nm. Figure 1c shows explicitly that the pitch distance (L as defined in the figure) is in the wide range of 200−500 nm and the zigzag angle is 120−130°, but the diameter of the helix (D) is uniformly 300 nm along the whole NW. We turned the TEM grid holder to rotate the NW around the axial direction. Figure 1d,e corresponds to the TEM images for its −30 and 30° rotations, respectively, showing the

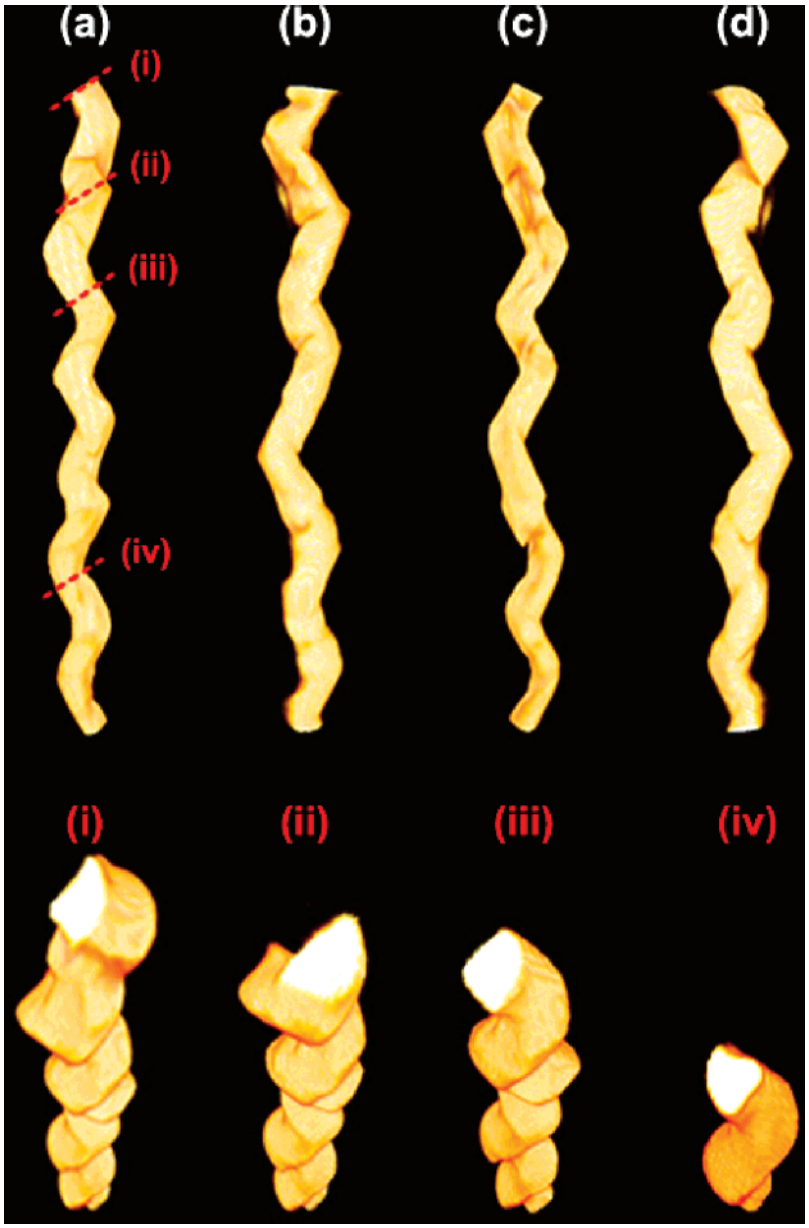

Figure 2. Images of the helical GaN NW obtained through tomographic 3D reconstruction; (a−d) correspond to a series of 0, 90, 180, and 270° rotations around the axial direction; (i−iv) images show the sliced view along the NWs (as marked in a), having the triangular cross section.

maintenance of the zigzagged morphology with the same *D* value. A series of TEM images for the 10° sequential rotations are shown in the Supporting Information, Figure S2.

The corresponding selected-area electron diffraction (SAED) pattern is shown in the insets. The zone axis is $[2\bar{1}\bar{1}0]$ for the 0° turn and $[01\bar{1}0]$ for the −30 and 30° turns. The [0001] axial direction remains the same for the rotation. This symmetric and periodic right-handed helix structure probably arises from the identical growth direction of the NW blocks (or units) that are directed toward the six equivalent directions of the hexagonal unit cell. The zigzagged direction, resulting from the shared direction of at least two blocks, can be identified using the edge parts ((i) and (ii)), as shown in the lower insets. At the $[2\bar{1}\bar{1}0]$ zone axis, the magnified images show the $[02\bar{2}3]$ and $[0\bar{2}23]$ directions. At the $[01\bar{1}0]$ zone axis, the NW clearly has the $[2\bar{1}\bar{1}2]$, $[\bar{2}112]$, and [0001] directions. However, the length of the blocks is very irregular, so that some of the shorter ones appear to be nearly collinear with the others (marked by the circles). This occurs as frequently as 1 per 4 or 5 zigzagged segments and causes an increase in the zigzag angle. Figure 1f−h displays the lattice-resolved images for the parts marked in Figure 1c−e, respectively, proving that this NW is entirely composed of perfect single-crystalline GaN nanocrystals. We observed the same zigzagged directions for other NWs, as shown in the Supporting Information, Figure S3.

Figure 2 displays the tomographic 3D reconstruction images of the helical GaN NW, as shown in Figure 1c−e, with panels a−d being the images for the 90° sequential turns. The corresponding movie is supplied in Supporting Information, Movie S1. The sliced views along the NW (as

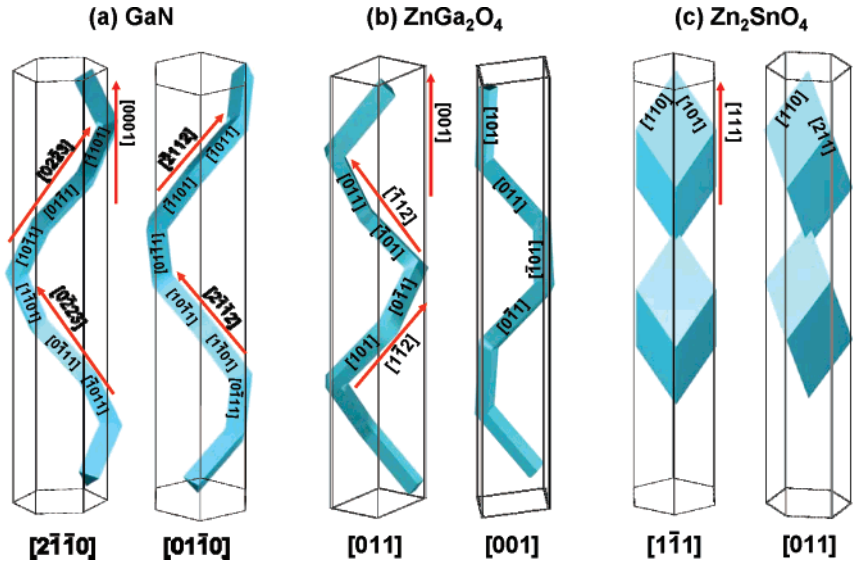

Figure 3. Schematic model constructed for the helical GaN and $ZnGa_2O_4$ NWs and zigzagged Zn_2SnO_4 NWs. (a) The GaN NW blocks have six equivalent $\langle 0\bar{1}11\rangle$ growth directions: $[\bar{1}101]$, $[01\bar{1}1]$, $[10\bar{1}1]$, $[1\bar{1}01]$, $[0\bar{1}11]$, and $[1011]$. These building blocks stack along the [0001] axial direction. The left and right images correspond to the views for the $[2\bar{1}\bar{1}0]$ and $[01\bar{1}0]$ zone axes, respectively. When the incident beam is projected at the $[2\bar{1}\bar{1}0]$ zone axis, the TEM image shows two $[02\bar{2}3]/[0\bar{2}23]$ zigzagged directions, resulting from the collinear three adjacent blocks. At the $[01\bar{1}0]$ zone axis, the two adjacent blocks become collinear and share the same growth direction, $[2\bar{1}\bar{1}2]$ and $[\bar{2}112]$, and the two blocks are aligned along the [0001] axial direction. (b) The blocks of the $ZnGa_2O_4$ nanosprings have four equivalent $\langle 011\rangle$ directions: [101], $[0\bar{1}1]$, $[\bar{1}01]$, and [011], and there is a 90° rotation between two adjacent blocks. The left and right images correspond to the views for the [011] and [001] zone axes, respectively. At the [011] zone axis, the TEM image shows that the two adjacent $[101]/[0\bar{1}1]$ or $[011]/[\bar{1}01]$ blocks become collinear and share the same growth direction of $[1\bar{1}2]$ or $[\bar{1}12]$. As the nanospring is rotated by 45°, two zigzagged directions are $[0\bar{1}1]$ and [011] when projected at the [001] zone axis. (c) The side edges of the rhombohedons have six equivalent $\langle 110\rangle$ directions: [110], $[1\bar{1}0]$, [101], $[10\bar{1}]$, $[01\bar{1}]$, and $[0\bar{1}1]$, and the axial direction is [111]. At the $[\bar{1}11]$ zone axis, the TEM image shows the [110] and [101] zigzagged directions and the [211] axial direction, which overlaps with the [111] axial direction (left image). As the NWs is rotated by 30°, the zone axis becomes [011] (right image). Then, one side edge coincides with the [211] direction, due to the collinear [011] and [101] directions.

marked in Figure 2a, i−iv), reveal the triangular cross-section. Supporting Information, Movie S2 provides the vertical-direction rotational view. The additional tomography data are supplied in the Supporting Information, Figure S4 and Movies S3 and S4.

On the basis of the assigned direction, we build a schematic model as shown in Figure 3a. The NW blocks stack along the [0001] axial direction. The blocks stack along the [0001] axial direction. They have six $\langle 0\bar{1}11\rangle$ growth directions: $[\bar{1}101]$, $[01\bar{1}1]$, $[10\bar{1}1]$, $[1\bar{1}01]$, $[0\bar{1}11]$, $[\bar{1}011]$. The angle between the $\langle 0\bar{1}11\rangle$ and $[01\bar{1}0]$ directions is 43.2°, as obtained from stereogram (Supporting Information, Figure S5). The triangular cross-section suggests that these NW blocks would be enclosed with $\pm(01\bar{1}\bar{2})$, $\pm(1\bar{1}01)$, and $(\pm(\bar{1}011)$ surfaces. When the incident beam is projected at the $[2\bar{1}\bar{1}0]$ zone axis, the TEM image shows two $[02\bar{2}3]$ and $[0\bar{2}23]$ zigzagged directions, resulting from the collinear three adjacent blocks (left image). As the NW is rotated by 30°, the two adjacent blocks become collinear and share the same growth direction, $[2\bar{1}\bar{1}2]$ and $[\bar{2}112]$, at the $[01\bar{1}0]$ zone axis (right image). At this zone axis, the two blocks line up along the [0001] axial direction.

Zigzagged GaN and coiled GaInN NWs were reported by other research groups, but the 3D structure of the helical GaN NWs has not previously been analyzed.[9,11] For the helical ZnO NWs, Wang and co-workers suggested a model in which the growth is led by the Zn-terminated (0001) front surface and the six equivalent $\langle 0\bar{1}11\rangle$ growth directions are formed to reduce the electrostatic interaction energy caused by the $\pm\{01\bar{1}1\}$ polar surfaces of the NWs.[5c] This model may be adopted for the present helical GaN NWs having the Ga (or N)-terminated $\pm(1\bar{1}01)$ and $\pm(\bar{1}011)$ polar side surfaces that attracted each other. Their controlled morphology is discussed in the Supporting Information.

We previously reported spinel-structure $ZnGa_2O_4$ nanosprings (right-handed), synthesized using ZnSe NWs as templates.[10] They have explicitly the $[1\bar{1}2]/[\bar{1}12]$ zigzagged directions (with a zigzag angle of 110°) at the [011] zone axis (Figure 4a and inset). They have a more uniform pitch length than the GaN NWs. When the nanospring is rotated by −45 or 45°, the $[0\bar{1}1]/[011]$ zigzagged directions (with a zigzag angle of 90°) are observed at the [001] zone axis (Figure 4b,c and insets). The [001] axial direction maintains along the whole length. A series of TEM images for the 10° rotation are shown in the Supporting Information, Figure S6. Figure 4d corresponds to the tomographic 3D reconstruction images, panels i−iv are the images for sequential 45° rotation, and v is for its top view, showing their square cross-section. The corresponding movies are displayed in Supporting Information, Movies S5 and S6. The schematic model is shown in Figure 3b. All these results confirm our previous structural assignment.

Zn_2SnO_4 NWs were synthesized using the vapor transport method, and their SEM image shows their diamond chainlike morphology (Figure 5a). The TEM image reveals that all of the NWs consist of linked rhombohedral nanocrystals (Figure

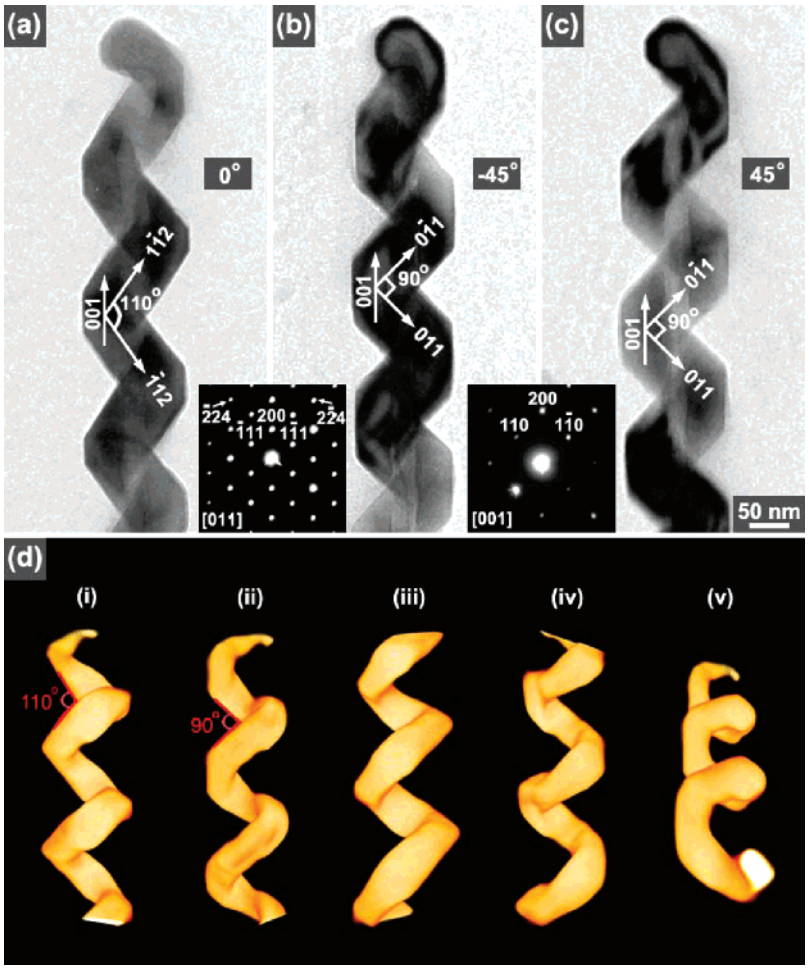

Figure 4. (a) The $ZnGa_2O_4$ nanosprings with a zigzag angle of 110°. Its corresponding SAED pattern, measured at the [011] zone axis, reveals the $[1\bar{1}2]$ and $[\bar{1}12]$ zigzagged directions and the uniform [001] axial direction along the whole length (inset). The TEM images for (b) −45° and (c) 45° turns around the axial direction show that the zigzag angle is 90°. Its corresponding SAED pattern, as shown in the inset, shows that the zone axis becomes [001] and the zigzagged direction matches $[0\bar{1}1]$ and [011]. (d) Tomographic reconstruction images of the $ZnGa_2O_4$ nanospring; (i−iv) images correspond to a series of 0, 45, 180, and 225° sequential rotations around the axial direction; (v) image shows the top view of the nanosprings. As it is rotated, the zigzag angle is changed from 110° (i and iii) to 90° (ii and iv).

5b). The energy-dispersive X-ray fluorescence (EDX), XRD, and XPS data confirm a face-centered cubic spinel structure, as shown in the Supporting Information, Figures S7 and S8. For a selected NW, the zigzag angle is 125° and the edge angle of the rhombohedral nanocrystals is 55°, as marked by the red-color lines (Figure 5c). The TEM image and SAED pattern (at the [011] zone axis) reveal the $[0\bar{1}1]$ and $[2\bar{1}1]$ zigzagged direction and the $[1\bar{1}1]$ wire axis (Figure 5d and inset). The lattice-resolved image confirms their single-crystalline nature (Figure 5e). Another NW was found to have a zigzag angle of 120° (Figure 5f). Its tip has an angle of 60° (Figure 5g). The SAED pattern at the $[\bar{1}11]$ zone axis indicates the [101] and [110] zigzagged directions and the [211] axial direction (inset). We measured a series of TEM images for the sequential rotation of another zigzagged NW (Supporting Information, Figure S9). As the NW is rotated by 30°, the zone axis changes from [011] to $[\bar{1}11]$, and the zigzag angle changes from 125 to 120°. Therefore, all of the NWs we observed have the same zigzagged structure. Figure 5h displays the tomographic 3D reconstruction images, and the corresponding movie is supplied in Supporting Information, Movies S7 and S8. Images i−iv correspond to sequential turns, showing the change of rhombohedral angle from 55 to 60°. The top view (v) reveals its rhombic-shaped cross-section.

A schematic model is shown in Figure 3c. We suggest that the six apexes of the rhombohedral blocks are directed toward the six equivalent ⟨110⟩ directions of the hexagonal units and the two apexes along the [111] axial direction. At the $[\bar{1}11]$ zone axis, the TEM image shows the [110]/[101] zigzagged directions and the [211] axial direction, which overlaps with the [111] direction (left image). As the NW is rotated by 30°, the zone axis becomes [011] (right image). Then, one side edge coincides with the [211] direction due to the collinear [110]/[101] directions. It is noteworthy that the assignment of the axial direction for such zigzagged NWs can often be incorrect when only the 2D projection image is used. Zigzagged Zn_2SnO_4 NWs were previously reported, commonly showing the [111] axial direction.[30−33] The zigzagged direction was observed to be [211] or [011], which is consistent with the present NWs. We also synthesized straight Zn_2SnO_4 NWs, having the [111] axial direction, as shown in the Supporting Information, Figure S10, and discussed their morphology control.

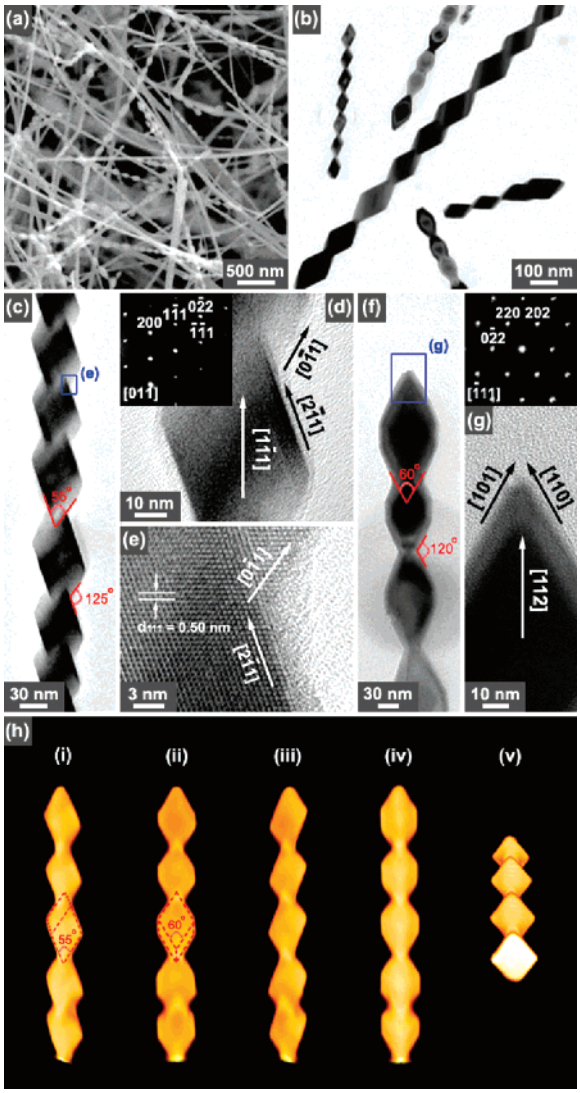

Figure 5. (a) SEM image showing diamond chainlike Zn_2SnO_4 NWs grown with high density on the substrates. (b) TEM image reveals that the NWs uniformly consist of linked rhombohedral-shaped nanocrystals. The diameter is modulated in the range of 10−100 nm. (c) TEM image of a selected NW shows the zigzag angle of 125° and the rhombohedral edge angle of 55°, as marked by the red-color lines. (d) Its magnified image for the linked part between the rhombohedrons and corresponding SAED pattern, measured at the [011] direction (inset) confirms that the zigzagged edges match to the $[2\bar{1}1]$ and $[0\bar{1}1]$ directions and the wire axis along the $[1\bar{1}1]$ direction. (e) Lattice-resolved TEM images showing that the distance between the (111) planes is 5.0 Å, which is consistent with that of the bulk Zn_2SnO_4 ($a = 8.650$ Å; JCPDS no. 24-1470). (f) TEM image of another zigzagged NW that consisted of chained hexagonal-shaped nanocrystals with a zigzag angle of 120°. (g) Magnified TEM image of the tip part and its corresponding SAED pattern (inset), measured at the $[\bar{1}11]$ zone axis, confirm the [110] and [101] directions along the zigzagged side edges and the [211] direction along the wire axis. The edge angle of the rhombohedral nanocrystals (as marked by the red-color lines) is exactly 60°. (h) Tomographic 3D reconstruction images of the Zn_2SnO_4 zigzagged NWs; a series of images for (i) 0°, (ii) 90°, (iii) 180°, and (iv) 270° sequential rotations around the axial direction. The (i)/(iii) images show the rhombohedral nanocrystals having an edge angle of 55° and a zigzag angle of 125°. The (ii)/(iv) images show that the edge angle of nanocrystals was changed to 60° by the rotation, and the zigzag angle becomes 120°. The (v) image reveals the cross section of the rhombohedral nanocrystals.

In summary, tomographic reconstruction and HRTEM images were used to characterize the unique 3D structures of right-handed helical GaN NWs that consist of six equivalent $\langle 0\bar{1}11 \rangle$ growth directions with the [0001] axial direction. We also present the tomography data for $ZnGa_2O_4$ nanosprings, having four equivalent $\langle 011 \rangle$ growth directions with the axial [001] direction. Zigzagged Zn_2SnO_4 NWs consisting of rhombohedral shaped nanocrystals in which the side edges match the six equivalent $\langle 110 \rangle$ directions and the axial direction is [111] were also studied. Therefore, we suggest that tomographic 3D construction allows for precise structure analysis, particularly for helical/zigzagged 1D nanostructures.

Acknowledgment. This work was supported by the KRF (Project No. R14-2004-033-01003-0; R02-2004-000-10025-0; 2004-015-C00125). The SEM, TEM (or HVEM), XRD, and XPS measurements were performed at the Basic Science Research Center. The experiments at the PLS were supported in part by MOST and POSTECH.

Supporting Information Available: Movies S1−S6. Experimental, growth mechanism, and additional TEM/tomography/XRD/XPS/EDX data of GaN, $ZnGa_2O_4$, and Zn_2SnO_4 NWs. This material is available free of charge via the Internet at http://pubs.acs.org.

References

(1) (a) Hu, J.; Odom, T. W.; Lieber, C. M. *Acc. Chem. Res.* **1999**, *32*, 435. (b) Gudiksen, M. S.; Lauhon, L. J.; Wang, J.; Smith, D. C.; Lieber, C. M. *Nature (London)* **2002**, *415*, 617. (c) Duan, X.; Huang, Y.; Agarwal, R.; Lieber, C. M. *Nature (London)* **2003**, *421*, 241.

(2) (a) Amelinckx, S.; Zhang, X. B.; Bernaerts, D.; Zhang, X. F.; Ivanov, V.; Nagy, J. B. *Science* **1994**, *265*, 635. (b) Chen, X.; Zhang, S.; Dikin, D. A.; Ding, W.; Ruoff, R. S.; Pan, L.; Nakayama, Y. *Nano Lett.* **2003**, *3*, 1299. (c) Bajpai, V.; Dai, L.; Ohashi, T. *J. Am. Chem. Soc.* **2004**, *126*, 5070. (d) Poggi, M. A.; Boyles, J. S.; Bottomley, L. A.; McFarland, A. W.; Colton, J. S.; Nguyen, C. V.; Stevens, R. M.; Lillehei, P. T. *Nano Lett.* **2004**, *4*, 1009. (e) Volodin, A.; Buntinx, D.; Ahlskog, M.; Fonseca, A.; Nagy, J. B.; Van Haesendonck, C. *Nano Lett.* **2004**, *4*, 1775.

(3) (a) Tang, Y. H.; Zhang, Y. F.; Wang, N.; Lee, C. S.; Han, X. D.; Bello, I.; Lee, S. T. *J. Appl. Phys.* **1999**, *85*, 7981. (b) Zhang, H.-F.; Wang, C.-M.; Buck, E. C.; Wang, L.-S. *Nano Lett.* **2003**, *3*, 577.

(4) (a) Zhang, H.-F.; Wang, C.-M.; Wang, L.-S. *Nano Lett.* **2002**, *2*, 941. (b) Zhang, D.; Alkhateeb, A.; Han, H.; Mahmood, H.; Mcllroy, D. N.; Norton, M. G. *Nano Lett.* **2003**, *3*, 983.

(5) (a) Kong, X. Y.; Wang, Z. L. *Nano Lett.* **2003**, *3*, 1625. (b) Kong, X. Y.; Ding, Y.; Yang, R.; Wang, Z. L. *Science* **2004**, *303*, 1348. (c) Yang, R.; Ding, Y.; Wang, Z. L. *Nano Lett.* **2004**, *4*, 1309. (d) Hughes, W. L.; Wang, Z. L. *J. Am. Chem. Soc.* **2004**, *126*, 6703. (e) Gao, P. X.; Ding, Y.; Mai, W.; Hughes, W. L.; Lao, C.; Wang, Z. L. *Science* **2005**, *309*, 1700. (f) Gao, P. X.; Wang, Z. L. *Small* **2005**, *1*, 945. (g) Gao, P. X.; Mai, W.; Wang, Z. L. *Nano Lett.* **2006**, *6*, 2536.

(6) Zhan, J.; Bando, Y.; Hu, J.; Xu, F.; Golberg, D. *Small.* **2005**, *1*, 883.

(7) Duan, J.; Yang, S.; Liu, H.; Gong, J.; Huang, H.; Zhao, X.; Zhang, R.; Du, Y. *J. Am. Chem. Soc.* **2005**, *127*, 6180.

(8) Duan, J. H.; Yang, S. G.; Liu, H. W.; Gong, J. F.; Huang, H. B.; Zhao, X. N.; Zhang, R.; Du, Y. W. *J. Phys. Chem. B* **2005**, *109*, 3701.

(9) Zhou, X. T.; Sham, T. K.; Shan, Y. Y.; Duan, X. F.; Lee, S. T.; Rogenberg, R. A. *J. Appl. Phys.* **2005**, *97*, 104315.

(10) Bae, S. Y.; Lee, J.; Jung, H. S.; Park, J.; Ahn, J. -P. *J. Am. Chem. Soc.* **2005**, *127*, 10802.

(11) Cai, X. M.; Leung, Y. H.; Cheung, K. Y.; Tam, K. H.; Djurišić, A. B.; Xie, M. H.; Chen, H. Y.; Gwo, S. *Nanotechnology* **2006**, *17*, 2330.

(12) Moore, D.; Ding, Y.; Wang, Z. L. *Angew. Chem., Int. Ed.* **2006**, *45*, 5150.

(13) Zhang, L.; Ruh, E.; Grützmacher, D.; Dong, L.; Bell, D. J.; Nelson, B. J.; Schönenberger, C. *Nano Lett.* **2006**, *6*, 1311.
(14) Yu, D.; Wu, J.; Gu, Q.; Park, H. *J. Am. Chem. Soc.* **2006**, *128*, 8148.
(15) He, Y.; Fu, J.; Zhang, Y.; Zhao, Y.; Zhang, L.; Xia, A.; Cai, J. *Small* **2007**, *3*, 153.
(16) (a) Shen, G. Z.; Bando, Y.; Zhi, C. Y.; Yuan, X. L.; Sekiguchi, T.; Golberg, D. *Appl. Phys. Lett*. **2006**, *88*, 243106. (b) Shen, G.; Bando, Y.; Liu, B.; Tang, C.; Golberg, D. *J. Phys. Chem. B* **2006**, *110*, 20129.
(17) Bell, D. J.; Dong, L.; Nelson, B. J.; Golling, M.; Zhang, L.; Grützmacher, D. *Nano Lett.* **2006**, *6*, 725.
(18) Kesapragada, S. V.; Victor, P.; Nalamasu, O.; Gall, D. *Nano Lett.* **2006**, *6*, 854.
(19) Zhai, T.; Gu, Z.; Yang, W.; Zhang, X.; Huang, J.; Zhao, Y.; Yu, D.; Fu, H.; Ma, Y.; Yao, J. *Nanotechnology* **2006**, *17*, 4644.
(20) Nath, M.; Parkinson, B. A. *J. Am. Chem. Soc.* **2007**, *129*, 11302.
(21) Möbus, G.; Doole, R. C.; Inkson, B. J. *Ultramicroscopy* **2003**, *96*, 433.
(22) (a) Thomas, J. M.; Midgley, P. A. *Chem. Comm.* **2004**, 1253. (b) Thomas, J. M.; Midgley, P. A.; Yates, T. J. V.; Barnard, J. S.; Raja, R.; Arslan, I.; Weyland, M. *Angew. Chem., Int. Ed.* **2004**, *43*. 6745. (c) Arslan, I.; Yates, T. J. V.; Browning, N. D.; Midgley, P. A. *Science* **2005**, *309*, 2195. (d) Gass, M. H.; Koziol, K. K. K.; Windle, A. H.; Midgley, P. A. *Nano Lett.* **2006**, *6*, 376. (e) Hungria, A. B.; Raja, R.; Adams, R. D.; Captain, B.; Thomas, J. M.; Midgley, P. A.; Golovko, V.; Jonhson, B. F. G. *Angew. Chem., Int. Ed.* **2006**, *45*. 4782. (f) Midgley, P. A.; Ward, E. P. W.; Hungría, A. B.; Thomas, J. M. *Chem. Soc. Rev.* **2007**, *36*, 1477.
(23) (a) Koster, A. J.; Ziese, U.; Verkleij, A. J.; Janssen, A. H.; de Jong, K. P. *J. Phys. Chem. B* **2000**, *104*, 9368. (b) Janssen, A. H.; Yang, C.-M.; Wang, Y.; Schüth, F.; Koster, A. J.; de Jong, K. P. *J. Phys. Chem. B* **2003**, *107*, 10552. (c) de Jong, K. P.; van den Oetelaar, L. C. A.; Vogt, E. T. C.; Eijsbouts, S.; Koster, A. J.; Friedrich, H.; de Jongh, P. E. *J. Phys. Chem. B* **2006**, *110*, 10209.
(24) Kanaras, A. G.; Sönnichsen, C.; Liu, H.; Alivisatos, A. P. *Nano Lett.* **2005**, *5*, 2164.
(25) (a) Bae, A.-H.; Numata, M.; Hasegawa, T.; Li, C.; Kaneko, K.; Sakurai, K.; Shinkai, S. *Angew. Chem., Int. Ed.* **2005**, *44*. 2030. (b) Kaneko, K.; Inoke, K.; Freitag, B.; Hungria, A. B.; Midgley, P. A.; Hansen, T. W.; Zhang, J.; Ohara, S.; Adschiri, T. *Nano Lett.* **2007**, *7*, 421.
(26) Yoshizawa, N.; Tanaike, O.; Hatori, H.; Yoshikawa, K.; Kondo, A.; Abe, T. *Carbon* **2006**, *44*, 2558.
(27) Ersen, O.; Werckmann, J.; Houlle, M.; Ledoux, M.-J.; Pham-Huu, C. *Nano Lett.* **2007**, *7*, 1898.
(28) Park, J.-B.; Lee, J. H.; Choi, H.-R. *Appl. Phys. Lett.* **2007**, *90*, 093111.
(29) Guckenberger, R. *Ultramicroscopy* **1982**, *9*, 167.
(30) (a) Wang, J. X.; Xie, S. S.; Gao, Y.; Yan, X. Q.; Liu, D. F.; Yuan, H. J.; Zhou, Z. P.; Song, L.; Liu, L. F.; Zhou, W. Y.; Wang, G. *J. Cryst. Growth* **2004**, *267*, 177. (b) Chen, H.; Wang, J.; Yu, H.; Yang, H.; Xie, S.; Li, J. *J. Phys. Chem. B* **2005**, *109*, 2573.
(31) Jie, J.; Wang, G.; Han, X.; Fang, J.; Yu, Q.; Liao, Y.; Xu, B.; Wang, Q.; Hou, J. G. *J. Phys. Chem. B* **2004**, *108*, 8249.
(32) Li, Y.; Ma, X. L. *Phys. Status Solidi A* **2005**, *202*, 435.
(33) Jeedigunta, S.; Singh, M. K.; Kumar, A.; Shamsuzzoha, M. *J. Nanosci. Nanotechnol.* **2007**, *7*, 486.

NL072829I